Received: 10 December 2018 | Revised: 22 January 2019 | Accepted: 1 April 2019

DOI: 10.1002/aoc.4965

FULL PAPER

WILEY Applied Organometallic Chemistry

Synthesis, structural characterization and DNA binding affinity of new bioactive nano-sized transition metal complexes with sulfathiazole azo dye for therapeutic applications

Fawaz A. Saad[1] | Hoda A. El-Ghamry[1,2] | Mohammed A. Kassem[1,3]

[1] Department of Chemistry, Faculty of Applied Science, Umm Al-Qura University, Makkah, Saudi Arabia

[2] Chemistry Department, Faculty of Science, Tanta University, Tanta, Egypt

[3] Chemistry Department, Faculty of Science, Benha University, Benha, Egypt

Correspondence
Hoda El-Ghamry, Department of Chemistry, Faculty of Applied Science, Umm Al-Qura University, Makkah, Saudi Arabia.
Email: helghamrymo@yahoo.com

Funding information
King Abdulaziz City for Science and Technology (KACST), Grant/Award Number: 37-175

The azo dye ligand 4-(5-chloro-2-hydroxyphenylazo)-*N*-thiazol-2-ylbenzenesulfonamide (H_2L) formed by the coupling reaction of sulfathiazole and *p*-chlorophenol was synthesized and characterized using elemental analysis and Fourier transform infrared (FT-IR) as well as UV–visible spectra. Nano-sized divalent Cu, Co, Ni, Mn and Zn complexes of the synthesized azo dye ligand were prepared and investigated using various spectroscopic and analytical techniques. Elemental and thermal analyses indicated the formation of the Cu(II), Ni(II) and Mn(II) complexes in a molar ratio of 1:2 (L:M) while Co(II) and Zn(II) complexes exhibited a 1:1 (M:L) ratio. FT-IR spectral studies confirmed the coordination of the ligand to the metal ions through the phenolic hydroxyl oxygen, azo nitrogen, sulfonamide oxygen and/or thiazole nitrogen. The geometric arrangements around the central metal ions were investigated applying UV–visible and electron spin resonance spectra, thermogravimetric analysis and molar conductance measurements. X-ray diffraction patterns revealed crystalline nature of H_2L and amorphous nature of all synthesized complexes. Transmission electron microscopy images confirmed nano-sized particles and their homogeneous distribution over the complex surface. Antibacterial, antifungal and antitumour activities of the investigated complexes were screened compared with familiar standard drugs to confirm their potential therapeutic applications. The Cu(II) complex showed IC_{50} of 3.47 μg ml^{-1} (5.53 μM) against hepatocellular carcinoma cells, which means that it is a more potent anticancer drug compared with the standard cisplatin (IC_{50} = 3.67 μg ml^{-1} (12.23 μM)). Furthermore, the Co(II), Ni(II), Cu(II) and Zn(II) complexes displayed IC_{50} greater than that of an applied standard anticancer agent (5-flurouracil) towards breast carcinoma cells. Hence, these complexes can be considered as promising anticancer drugs. The mode of binding of the complexes with salmon serum DNA was determined through electronic absorption titration and viscosity studies.

KEYWORDS
anticancer, characterization, DNA binding, nano-sized complexes, sulfthiazole

1 | INTRODUCTION

It is well known that sulfonamide derivatives result from the interchanges of different functional groups while retaining the essential structural merit of sulfonamide moiety (—SO_2—NH—), and can display a wide range of curative and pharmacological activities.[1,2] Depending on the great ability of sulfonamides to coordinate with metal ions through diverse manners, a great number of scientific of publications have been concentrated on sulfonamide complexes.[3,4] The tendency of sulfonamides to act as ligands is supposedly attributable to the acidic behaviour of the —SO_2—NH— site resulting in the formation of anionic donor supported with the presence of O, N and/or S atoms in the adjoining heterocyclic ring. Such thematic environments grant the stereochemical demands for fulfilling assorted arrangements like monomeric, dimeric and polymeric structures.[5] The aromatic amino group which is the other requisite part in sulfonamide compounds is the major source of the chemical variety of this class of compounds which enable them to act as good coordination centres. However, what appears more important is that this part is a reactive site for chemical modifications of sulfonamide ligands to acquire an immense number of complexes of biological importance. Heterocyclic azo dyes occupy a great position in the growth of coordination chemistry. The prominence of such compounds arises from their biological effectiveness in addition to their analytical applications.[6] On the other hand, derivatives of heterocyclic azo dyes have been utilized to settle the depressed oxidation states of diverse transition metal elements.[7] Most significant is that sulfonamide and azo dye derivatives of sulfonamide were found to have biologically varying antitubercular, antimalarial and anticancer properties.[8] Additionally, the azo dye derivatives of sulfonamide compounds are applicable as potential ligands for numerous metals.[9,10] Such metal complexes exhibited tremendous utility in dying processes and bio-systems as well as analytical detection of several metallic elements in real samples.[11] Along with sulfonamide derivatives, sulfathiazole (4-amino-*N*-2-thiazolylbenzenosulfonamide) is considered one of the most important clinically used compounds.[12] Also, binuclear and polynuclear metal complexes have attracted much attention attributable to their numerous implementations in bio-systems,[13,14] and material sciences,[15] besides their unique spectral and magnetic properties.[16] Also, the interaction of DNA with small molecules is a promising field of research as it considered as an overlapping area between chemistry and biology.[17,18] Such small molecules interact with DNA through weak forces such as π-stacking reactions which are usually accompanied with intercalation of the aromatic (planar) constituent between base pairs of the different types of DNA, van der Waals forces and hydrogen bonding as well as interactions of functionalities bound through the cavity of the DNA helix.[19] Studies aimed at the design of conformation- and site-specified reagents supply rationale for novel drug styling as well as improved susceptible chemical probes for the structure of nucleic acids. Recently, the interactions between nucleic acids and transition metal complexes have attracted great attention, because of their importance in the evolution of unprecedented reagents for medical science and biotechnology.[20]

Keeping in mind all these considerations, we report here the synthesis, structural characterization, DNA binding affinity and biological efficacy of a new series of mono and homo binuclear transition metal complexes with sulfathiazole azo dye (H_2L) for prospective chemotherapeutic uses. The operative and active coordination sites in H_2L and the geometrical configurations of the complexes were investigated applying elemental and thermal analyses, Fourier transform infrared (FT-IR), electron spin resonance (ESR) and electronic absorption spectroscopies, X-ray diffraction (XRD), transmission electron microscopy (TEM) as well as various physical measurements. The mode of binding of the studied compounds with DNA was determined applying electronic absorption titration and viscosity techniques. This is due to the great importance of studying the interaction of metal complexes with nucleic acids in developing new reagents for biotechnological and medicinal applications. Also, the investigated compounds were screened *in vitro* for their antitumour and antimicrobial activities to evaluate their potential therapeutic activities as new therapeutic agents.

2 | EXPERIMENTAL

2.1 | Preparation of sulfathiazole azo dye ligand

The azo dye ligand was prepared using to the following procedures. A suspension of 4-amino-*N*-(1,3-thiazol-2-yl) benzenesulfonamide (2.55 g, 0.001 mol) in equal volumes of HCl and water (15 ml) was warmed to 80°C until complete dissolution. The resulting clear solution was cooled below 5°C and diazotized using $NaNO_2$ (1.5 g) dissolved in 15 ml of water. To a solution of *p*-chlorophenol (1.29, 0.001 mol) in water containing 1.6 g of NaOH, the obtained diazonium salt was added in the course of 30 min at 0°C. The addition process took place dropwise with continuous stirring. The precipitate was filtered off, and then washed several times. The produced sulfathiazole azo dye ligand H_2L (Figure 1) was recrystallized several times from ethanol.

2.2 | Synthesis of nano-sized metal complexes with sulfathiazole azo dye ligand

Nano-sized transition metal complexes were synthesized according to the well-known reflux–precipitation method. Amounts of 0.001 or 0.002 mol of various transition metal salt solutions (0.002 mol (0.34 g) of $CuCl_2{\cdot}2H_2O$, 0.001 mol (0.237 g) of $CoCl_2{\cdot}6H_2O$, 0.002 mol (0.474 g) of $NiCl_2{\cdot}6H_2O$, 0.002 mol (0.394 g) of $MnCl_2{\cdot}4H_2O$, 0.001 mol (0.287 g) of $ZnSO_4{\cdot}7H_2O$) dissolved in 30 ml of 50% (v/v) H_2O–C_2H_5OH mixture were added to an ethanolic solution of H_2L (0.001 mol (0.394 g) in 40 ml of C_2H_5OH), drop by drop with constant stirring. The obtained solutions (from mixing) were heated for 10–14 h using a water bath. The metal chelates formed (after addition of a few drops of triethylamine) during the reaction were isolated by filtration followed by washing with ethanol and ether. Then, the prepared metal complexes were dried in a vacuum over $CaCl_2$ (anhydrous) and their purities were confirmed by TLC.

2.3 | Analytical and physical measurements

Elemental microanalyses for C, H and N contents were performed using a 2400 CHN elemental analyser (PerkinElmer). A Sherwood magnetic susceptibility balance was applied to obtain the room temperature magnetic moment values of the complexes. Electronic absorption spectra of all compounds were performed applying the Nujol mull technique using a Shimadzu spectrometer (model UV-3600). ^{1}H NMR spectra were obtained using a Mercury Oxford NMR 300 Hz spectrophotometer using tetramethylsilane as internal standard after dissolving the samples in deuterated dimethylsulfoxide (DMSO-d_6). The molar conductance was determined in DMF solvent (10^{-3} M) using a JENWAY (model 4070) conductance bridge. A Bruker Tensor 27 FT-IR spectrophotometer was used to measure FT-IR spectra as KBr discs within the range 400–4000 cm^{-1}. The X-band powder ESR spectrum of the Cu(II) complex was obtained with a Jeol JES-RE1X EPR spectrometer (Alexandria University, ν = 9.435 GHz). A GNR X-ray diffractometer (APD2000PRO) was used for recording the XRD patterns of the complexes, applying Cu Kα_1 radiation using a graphite monochromator (at 0.03° min^{-1} scanning rate). Thermogravimetric analysis (TGA) of the complexes was accomplished using a Shimadzu TG-50 thermal analyser, in the presence of nitrogen as atmosphere using a 10 C min^{-1} heating rate.

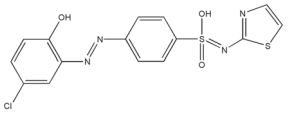

FIGURE 1 Molecular structure of the prepared ligand, H_2L

2.4 | Antitumour assays

The antitumour activity of the compounds under study was tested against hepatocellular carcinoma cells compared with the standard drug cisplatin and breast carcinoma cells compared with 5-flurouracil as standard agent. MCF-7 cells (human breast cancer cell line) and HepG-2 cells (human hepatocellular carcinoma cell line) were provided by VACSERA Tissue Culture Unit. The cells were proliferated in Dulbecco's modified Eagle's medium containing 10% foetal bovine serum (heat-inactivated), L-glutamine (1%), buffer (HEPES) and gentamycin (50 μg ml^{-1}). Whole cells were preserved at 37°C in a moistened atmosphere with CO_2 (5%) and were sub-cultured (two times a week). For anticancer activity determination, the cells were cultured in 100 μl of growth medium in a 96-well plate at a cell concentration of 1×10^4 cells per well. Fresh medium containing various concentrations of the examined component was added after 24 h of cultivation. Series of twofold dilutions of the tested component were added to confluent cell monolayers distributed into 96-well, flat-bottomed microtitre plates (Falcon, NJ, USA) applying a multichannel pipette. The microtitre plates were developed at 37°C in a humidified incubator with CO_2 (5%) for 48 h. For every concentration of the examined sample, three wells were utilized. Control cells were developed without examined sample and without or with DMSO. The small DMSO percentage existing (maximal 0.1%) in the wells had no influence on the experiment. After cell incubation (at 37°C), different sample concentrations were placed, and the incubation was continued (for 24 h) and the yield of viable cells was counted using a colorimetric method. After the ending of the incubation time, media were sprinkled and 1% crystal violet solution was added to all wells (for 30 min at least). The stain was removed and the plates were washed with tap water until the extra stain was removed. Glacial CH_3COOH (30%) was then added to all wells and fully mixed, and the absorbance was determined after gently shaking with a microplate reader (TECAN, Inc.) at 490 nm. All results were corrected for background absorbance of wells without applying stain. Treated samples were compared with the cell control in the absence of the examined material. Each experiment was repeated three times. The cell cytotoxic influence of each tested sample was determined. The

optical density was determined using a microplate reader (SunRise, TECAN, Inc., USA) to determine the viable cell number and the viability percentage was computed as $[1 - (ODt/ODc)] \times 100\%$, where ODc is the mean optical density of untreated cells and ODt refers to the mean optical density of wells treated with the examined specimen. A plot relating the surviving cells and tested sample concentration was made to get the survival curve of each tumour cell line after treatment with the examined sample. IC_{50} (50% inhibitory concentration), the concentration required to cause toxic effects in 50% of intact cells, was determined from graphic plots of the dose–response curve for each concentration applying GraphPad Prism software (San Diego, CA, USA).[21,22]

2.5 | Antimicrobial evaluation

The synthesized ligand and complexes were separately investigated against a plate of Gram-negative and Gram-positive bacterial strains and fungi. Antimicrobial tests were conducted applying the diffusion agar technique. Pathological bacteria, 1×10^6 CFU ml^{-1} yeast and 1×10^4 spores ml^{-1} fungi were distributed on nutrient agar and Sab. dextrose agar, successively.[23] After solidification, 6 mm (diameter) wells were made in the solidified agar and loaded with 100 μl of examined specimen solution provided by dissolving 20 mg of the test component in DMSO. Then, the inoculated dishes were incubated for 48 h at 28°C for fungi and 24 h at 37°C for bacteria. Negative reference was tested applying DMSO used to dissolve the tested samples. Ketoconaz was applied as standard for fungi and gentamycin as standard for bacteria. After incubation, antimicrobial activity was estimated by determining the inhibition zone for the test organisms.

2.6 | DNA binding mode investigation

Because of the enormous significance of investigating the type of interaction between chemical compounds and DNA for the improvement of modern reagents for medical science and biotechnology, the mode of binding between salmon serum DNA (SS-DNA) and the characterized compounds was investigated using two methods.[24] The first method involved absorption spectroscopic titration in which increasing amounts of DNA solution were added to a specified concentration of the compound of interest and measuring the electronic spectra for all solutions. The intrinsic binding constant (K_b) was computed. Using the binding constant values, we can evaluate whether the binding mode with DNA is intercalative or non-intercalative.[24] The second method was based on viscosity studies, which offer inclusive precision to any change in the length of DNA. In this method, DNA specific viscosity was determined applying several concentrations of the material of interest while fixing the concentration of DNA. The obtained results were represented as $(\eta/\eta_0)^{1/3}$ versus [compound]/[DNA] (mole ratio), where η is the viscosity of DNA in the presence of examined material and η_0 is the viscosity of DNA in the absence of the examined material. Viscosity measurement of DNA can be regarded as a conventional way that is utilized in order to investigate the mode of binding of DNA with compounds.

3 | RESULTS AND DISCUSSION

3.1 | Microanalytical results and molar conductance

The obtained data from elemental analysis of organic azo dye ligand H_2L and complexes **1**–**5** are in good agreement with the proposed molecular formulae (Table 1). The results confirm formation of 2:1 (M:L) stoichiometry for complexes **1**, **3** and **4** and 1:1 (M:L) for complexes **2** and **5**. The data from molar conductance determined in 10^{-3} M DMF solution were found to be within the range 13.1–27.9 Ω^{-1} cm^2 mol^{-1}. These values support the non-electrolytic character of the complexes.[25]

3.2 | ^{1}H NMR spectra

The ^{1}H NMR spectrum of H_2L (Figure 2) displayed two singlet bands at 12.90 and 10.91 ppm due to the hydrogen bonded OH protons of phenolic group and sufonamide moiety, respectively. The aromatic protons resonate as a multiplet at 6.77–8.69 ppm.[5] Furthermore, the ^{1}H NMR spectrum of the ligand showed a sharp singlet at 9.70 ppm which can be attributed to the NH proton. The appearance of this signal is explained by the tautomeric shift in the sulfonamide moiety shown below:

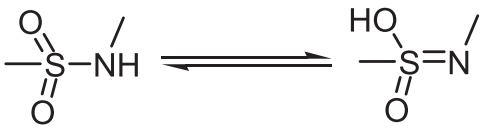

3.3 | FT-IR spectra and mode of bonding

For investigation the coordination sites in the ligand that participate in bond formation with the metal ions, the FT-IR spectra of complexes **1**–**5** are contrasted with that of the parent ligand (Figure 1S). The intrinsic peaks in the H_2L spectrum are used to assist in understanding.

TABLE 1 Microanalysis and some physical characteristics of H_2L and complexes **1–5**

Compound	Molecular formula (empirical formula)	Colour (molecular weight, g mol^{-1})	M.p. (°C) (yield, %)	Microanalysis: calcd (found)			
				C (%)	H (%)	N (%)	M (%)
H_2L	$C_{15}H_{11}ClN_4O_3S_2$	Yellow (394.86)	163 (83)	45.63 (45.58)	2.81 (2.81)	14.19 (14.31)	—
1	$[LCu_2Cl_2(H_2O)_2]$ ($C_{15}H_{13}Cl_3Cu_2N_4O_5S_2$)	Brown (626.87)	>300 (75)	28.74 (28.78)	2.09 (2.15)	8.94 (8.87)	20.27 (20.09)
2	$[LCoCl(H_2O)]2H_2O$ ($C_{15}H_{16}Cl_2CoN_4O_6S_2$)	Brown (542.28)	>300 (74)	33.22 (33.09)	2.97 (2.86)	10.33 (10.28)	10.87 (11.01)
3	$[LNi_2Cl_2(H_2O)_2]MeOH$ ($C_{16}H_{17}Cl_3N_4Ni_2O_6S_2$)	Brown (649.21)	>300 (69)	29.60 (29.52)	2.64 (2.59)	8.63 (8.68)	18.08 (18.75)
4	$[LMn_2Cl_2(H_2O)_2]$ ($C_{15}H_{15}Cl_3Mn_2N_4O_5S_2$)	Brown (609.65)	>300 (64)	29.55 (29.63)	2.15 (2.23)	9.19 (9.28)	18.02 (17.68)
5	$[LZnSO_4]H_2O$ ($C_{15}H13ClN_4O_8S_3Zn$)	Reddish brown (574.32)	>300 (84)	31.37 (31.60)	2.28 (2.35)	9.76 (10.04)	11.39 (11.52)

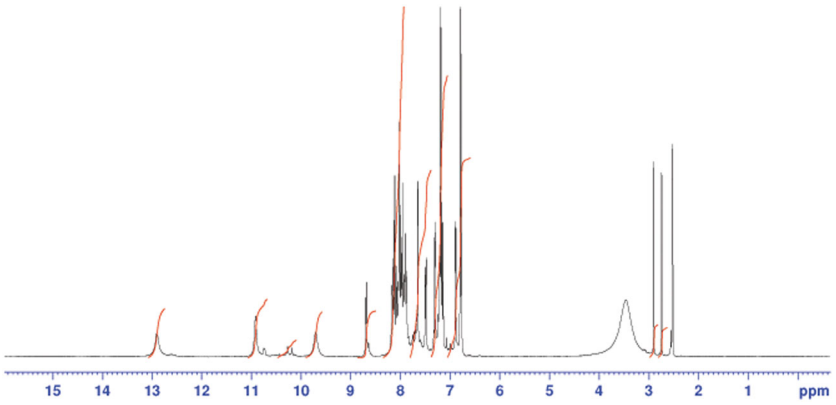

FIGURE 2 ^1H NMR spectrum of H_2L

Upon chelation, these peaks usually display alterations either in their positions, shapes and/or their intensities. Some of them vanish upon chelation. The FT-IR bands of importance for the synthesized H_2L and compounds **1–5** are listed in Table 2. For free ligand H_2L, the spectrum displayed a broad band centred at 3423 cm^{-1}, attributed to the stretching vibrations of intramolecular hydrogen bonded OH groups,[26] and a band appeared at 3231 cm^{-1} assigned to ν_{NH}. Spectra of all complexes showed broad bands within the 3419–3441 cm^{-1} range assigned to ν_{OH} of water molecules connected with the complexes. Also, the complexes exhibited weak bands at 783–807 cm^{-1} for $\delta(H_2O)$ of coordinated molecules.[27] The band appearing in the ligand spectrum at 1422 cm $^{-1}$ is assigned to $\nu_{N=N}$. These bands exhibited obvious shifts to higher wavenumbers by 18–34 cm^{-1} upon complex formation supporting the chelation towards metallic centres through the azo nitrogen atom. The ligand band appearing at 1212 cm^{-1} was assigned to ν_{C-O}. This band underwent upfield or downfield variation in the metal chelated spectra confirming the attachment of the α-position hydroxyl group in complex formation through proton displacement; except for complex **5**, in which the hydroxyl group attached to the metal centre. The band

TABLE 2 Assignments for diagnostically important bands in FT-IR spectra (cm^{-1}) for H_2L and complexes **1–5**

Compound	ν(OH)	ν(NH)	ν(C=N)	ν(N=N)	ν(C—O)	ν(M—O)	ν(M—N)
H_2L	3423	3231	1570	1422	1212	—	—
1	3433	3240	1592	1456	1232	514	441
2	3441	—	1594	1448	1225	568	445
3	3421	—	1593	1441	1237	570	447
4	3420	3242	1592	1445	1203	572	460
5	3419	—	1590	1440	1231	570	441

that appeared in the ligand spectrum at 1570 cm^{-1} was assignable to $\nu_{C=N}$ bond of thiazole ring. The shift in this band in the spectra of complexes **1**, **3** and **4** is due to participation in complex formation. With respect to complexes **2** and **5**, the change in this band is attributed to its involvement in hydrogen bond formation with the adjacent NH group. The non-ligand bands appearing in the complex spectra within 572–514 and 460–441 cm^{-1} ranges can be attributed to M—O and M—N stretching vibrations, respectively.[28]

3.4 | TGA and kinetic parameters

TGA is a helpful tool for providing evidence supporting the molecular structure of metal complexes,[29,30] through affording valuable information about their thermal features, thermal degradation stages, nature of intermediates and the residual products of their thermal decomposition steps.[31] It is important to determine the percentage and type of water and/or organic solvent molecules alongside the anionic groups associated with the metal ions. Based on these facts, solid complexes **1**–**5** were subjected to TGA. The successive thermal decomposition stages, types of intermediates, temperature ranges and different pyrolysis products, in addition to the found and theoretical calculated weight loss percentages in every degradation stage are presented in Table 1S and the TGA thermograms are shown in Figure 2S. From the TGA thermograms of complexes **1**–**5**, it was observed that the metal chelates decompose within three (complexes **2** and **4**) or four (complexes **1**, **3** and **5**) successive decomposition steps. Within the first step of decomposition, the lattice (complexes **2**, **3** and **5**) or coordinated (complexes **1** and **4**) solvent molecules (water or methanol) evaporate. The coordinated anions (chloride or sulfate) are lost with the second and third decomposition steps. Within the following steps of decomposition, the organic moiety is successively decomposed leaving behind the thermally stable metal oxide or pure metal as a final residue. The thermal decomposition of compound **3**, as an example, can be represented by the following schemes:

$$[LNi_2Cl_2(H_2O)_2]MeOH \xrightarrow[\text{-5.41 (}calcd.\text{ 4.92 \%)}]{\text{25-69 }^{o}\text{C}} [LNi_2Cl_2(H_2O)_2]$$

$$[LNi_2Cl_2(H_2O)_2] \xrightarrow[\text{-16.24(}calcd.\text{ 16.32 \%)}]{\text{69-295 }^{o}\text{C}} [LNi_2]$$

$$[LNi_2] \xrightarrow[\text{-42.42 (}calcd.\text{ 42.17 \%)}]{\text{295-448 }^{o}\text{C}} \text{Intermediate 1}$$

$$\text{Intermediate 1} \xrightarrow[\text{-18.75 (}calcd.\text{ 18.08 \%)}]{\text{727-742 }^{o}\text{C}} 2Ni$$

The TGA data for complexes **1**–**5** strongly support their proposed molecular compositions.

The kinetic parameters (order of reaction n, pre-exponential factor A and energy of activation ΔE) for the thermal degradation stages were evaluated applying the Coats–Redfern equation[32] (Figures 3 and 3S). The thermodynamic activation parameters (ΔH, ΔS and ΔG) were calculated using the following relationships:

$$\Delta H = \Delta E - RT$$

$$\Delta S = R[\ln(Ah/kT) - 1]$$

$$\Delta G = \Delta H - T\Delta S$$

where k is the Boltzmann constant and h is the Planck constant.

From the results listed in Table 3 we can deduce that the negative sign of entropies of activation (ΔS^*) indicates that the activated complex is more ordered than reactants and/or the decomposition reactions of the complexes are slower than normal.[33] The positive values of ΔH indicate endothermic decomposition processes.[34] It is also observed that the kinetics of the thermal decomposition stages of all complexes obeys, in most cases, zero- or first-order kinetics. The values of activation energies increase as the maximum temperature of decomposition increases indicating high stability of the complexes under investigation.

3.5 | UV–visible spectra and magnetic moments

UV–visible (electronic absorption) spectra are known as a significant tool in differentiation between various geometrical structures, square planar, octahedral and tetrahedral, of metal chelates. They are also a useful aid to investigate the coordination of ligand constituent atoms to metallic sites. The UV–visible spectra of the metal chelates were recorded by the Nujol mull technique within the range 200–800 nm. The Cu(II) chelate presented a broad band at 752 nm attributed to $^2B_{1g} \rightarrow {}^2A_{1g}$ transition, supporting a square planar geometrical arrangement around the Cu centre. A band appeared at 359 nm, assigned to n → π* transition, while the band appearing at 486 nm is due to ligand-to-metal charge transfer.[35] The recorded magnetic moment (room temperature) of the Cu(II) complex was determined to be 1.76 BM. This value lies near the range of the spin-allowed values expected for one unpaired electron (1.72 BM), supporting the obtained electronic spectral results.[36] For the Co(II) complex, two bands which were observed at the visible region at 533 and 715 nm, assigned to $^4A_2 \rightarrow {}^4T_1$ (υ_2) and $^4A_2 \rightarrow {}^4T_1(P)$ (υ_3) transitions, respectively, were

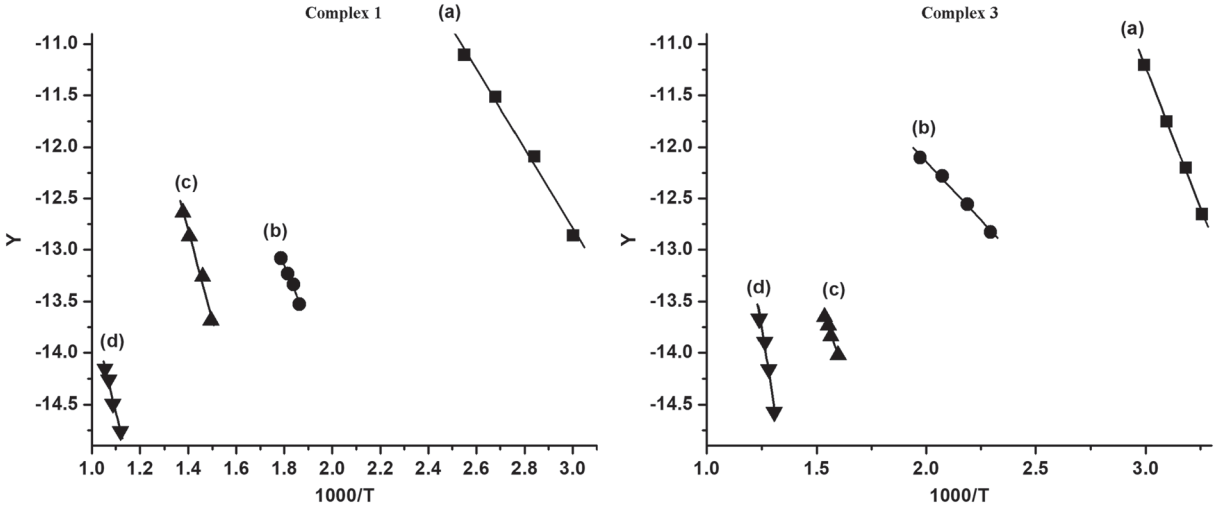

FIGURE 3 Coats–Redfern plots for complexes **1** and **3**. (a) First step, (b) second step, (c) third step and (d) fourth step, where $Y = [1 - (1 - \alpha)^{1-n}]/(1 - n)T^2$ for $n \neq 1$ or $Y = [\ln(1 - \alpha)]/T^2$ for $n = 1$

evidence for four-coordinate tetrahedral stereochemistry around the metal centre.[37] For the Co(II) complex, the magnetic moment value is 4.28 BM, which is greater than theoretical spin-only value for Co(II) complexes indicating the orbital participation of Co(II) complexes.[38] The spectrum of the Ni(II) complex displayed three absorption bands at 473, 576 and 738 nm corresponding to $^3T_1(F) \rightarrow {}^3T_1(P)$, $^3T_1(F) \rightarrow {}^3A_2(F)$ and $^3T_1(F) \rightarrow {}^3T_2(F)$ transitions that are consistent with Ni(II) tetrahedral complex. The value of magnetic moment measured for the Ni(II) complex was 3.41 BM, consistent with the tetrahedral structure of complex,[39] giving extra evidence for this proposal. The spectrum of the Mn(II) complex displayed two bands in the visible region at 420 and 587 nm assigned to $^6A_1 \rightarrow {}^4T_2(G)$ and $^6A_1 \rightarrow {}^4T_1(G)$ transitions, in agreement with tetrahedral geometry.[40] The Mn(II) complex has low magnetic moment value of 5.23 BM as a result of metal–metal interactions. Finally, for complex **5**, as a d^{10} system having no unpaired electrons, the spectrum of the Zn(II) complex displayed bands at 458 and 527 nm attributed to charge transfer transitions. The apparent changes in ligand bands are excellent proof for complex formation.[41] The electronic spectrum of the Zn(II) complex did not introduce any useful knowledge about its stereochemistry and the Zn(II) complex displayed diamagnetic character.

TABLE 3 Activation parameters (ΔH, ΔS^*, ΔG^*) for decomposition stages of complexes **1–5**

Complex	*n*	Step	*r*	*E**	ΔH^*	*A*	$-\Delta S^*$	ΔG^*
1	1	1st	0.995730	32.14492	29.13110	127012.7842	0.157141	86.09481
	1	2nd	0.992379	47.12241	42.56634	1080534.578	0.142777	120.8084
	1	3rd	0.9931606	71.59581	65.79264	184222.9018	0.159496	177.1215
	0	4th	0.9947711	79.87832	72.20035	5285074.578	0.133918	195.8741
2	1	1st	0.998263	18.418672	13.976918	202580699.2	0.0990533	66.89614
	1	2nd	0.996412	27.256068	24.165338	1021388.244	0.1400191	76.21745
	1	3rd	0.985270	99.233199	92.937422	96578.96891	0.1655434	218.2951
3	1	1st	0.996827	45.220508	15.061283	44516052.49	0.110595	67.09621
	1	2nd	0.992561	19.900176	14.774595	540710172.2	0.0920816	71.54288
	0	3rd	0.999274	18.97302	42.564185	336.1722858	0.2054302	108.1991
	1	4th	0.989802	111.58072	105.04799	6591.671536	0.1881699	252.9025
4	1	1st	0.990349	20.31587	15.524928	562098677.9	0.0911977	68.077608
	0.33	2nd	0.987279	71.978118	69.276068	0.048010458	0.279184	160.0109
	0	3rd	0.998258	84.701937	78.181683	339620.21	0.1553801	200.03849
5	1	1st	0.9772249	28.623573	25.609748	208607.9453	0.1530161	81.07809
	0.66	2nd	0.9037826	22.713336	18.801599	27577317.35	0.1145762	72.709685
	0	3rd	0.9899152	44.955321	39.551221	13366900.25	0.1232842	119.68592
	1	4th	0.9971191	165.5969	159.21383	1.093353349	0.2603449	359.0936

3.6 | ESR spectral studies

ESR measurement was accomplished for the Cu(II) complex using powder material at ambient temperature, which provided only a value of g_{eff} and does not give $g_{||}$ parallel and $g_{\perp}$ perpendicular values. As a result of the dipolar interaction from the ESR spectrum of a set of magnetic parameters, the spectrum exhibited a broadened feature without hyperfine splitting. Two anisotropic signals were perceived in the ESR spectrum of the Cu(II) complex (Figure 4). The profile of the ESR spectrum supported the proposed geometry of the Cu(II) complex and coincided with the data gained from magnetic and electronic spectral studies. The g_{eff} value was found to be 2.1321 BM. The observed positive deviation from the standard free electron value (2.0023) is attributed to the measurable covalent bonding modes between the investigated ligand and metal ions. Consequently, the metals interact with H_2L in the investigated complexes basically in covalent mode.[42]

Based on the data gained from microanalysis, TGA, FT-IR, ESR and electronic spectra supported with molar conductance and magnetic moment measurements, the bonding of H_2L to the metal ions and the structure of the investigated compounds can be proposed, as shown in Figure 5.

3.7 | XRD and TEM analyses

XRD is deemed to be one of the most useful techniques for obtaining structural microcrystalline information regarding the studied compounds.[43] Also, it is usually applied to provide an explicit view concerning the lattice dynamics of compounds in the solid phase.[44] Hence, the

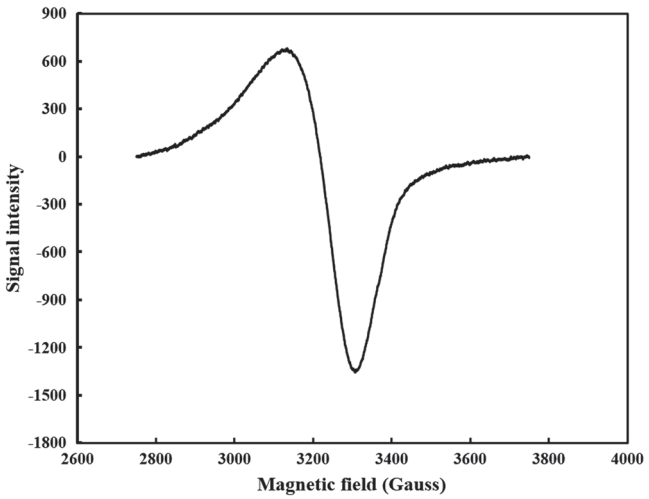

FIGURE 4 ESR spectral band of nanosized Cu(II) complex (**1**)

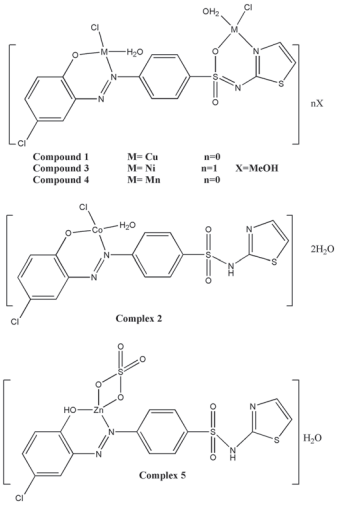

FIGURE 5 Structures of nano-sized divalent Cu, Co, Ni, Mn and Zn complexes

XRD patterns of the ligand (H_2L) and complexes **1**–**5** were obtained in the $0° < 2\theta < 90°$ range of scattering angle. The diffraction pattern of free ligand is very different compared with those of the corresponding metal complexes (Figures 6 and 4S), supporting the formation of the complexes. The ligand pattern indicates good crystallinity whereas complexes **1**–**5** were found to be relatively amorphous. This can be attributed to infrequent configuration for solid frameworks throughout the precipitation process. Often, if the solution is cooled rapidly enough or the reaction is fast, the precipitated compound will solidify in an amorphous state. Furthermore, some solids are found intrinsically amorphous since their constituents are not capable of giving a perfect fit in a crystalline lattice. This deprives one of the opportunity for computing the crystallite sizes or *d*-spacing inside the lattice giving insight about the solid complexes. The amorphous nature of the compounds reflected the very small size for the aggregates which is easily found within the nanometre range, which can be investigated applying the TEM technique.[45]

TEM is usually applied to elucidate diverse interesting nano-sized metal complexes.[46] It is a general implemented technique utilized to investigate the particle size and shape of solid materials. High-resolution TEM images were obtained for complexes **1**–**5** (Figures 7 and 5S). We used TEM in order to acquire evident knowledge concerning the particle size, surface morphology, microstructure and homogeneity for the metal complexes. The micrographs show various particle shapes in nanocrystalline matrices. They display uniform and homogeneity of surface morphology for all scrutinized samples. Likewise, the images show the uniformity and propinquity among the forms of particles supporting the occurrence of identical matrices. The presence of highly symmetrical

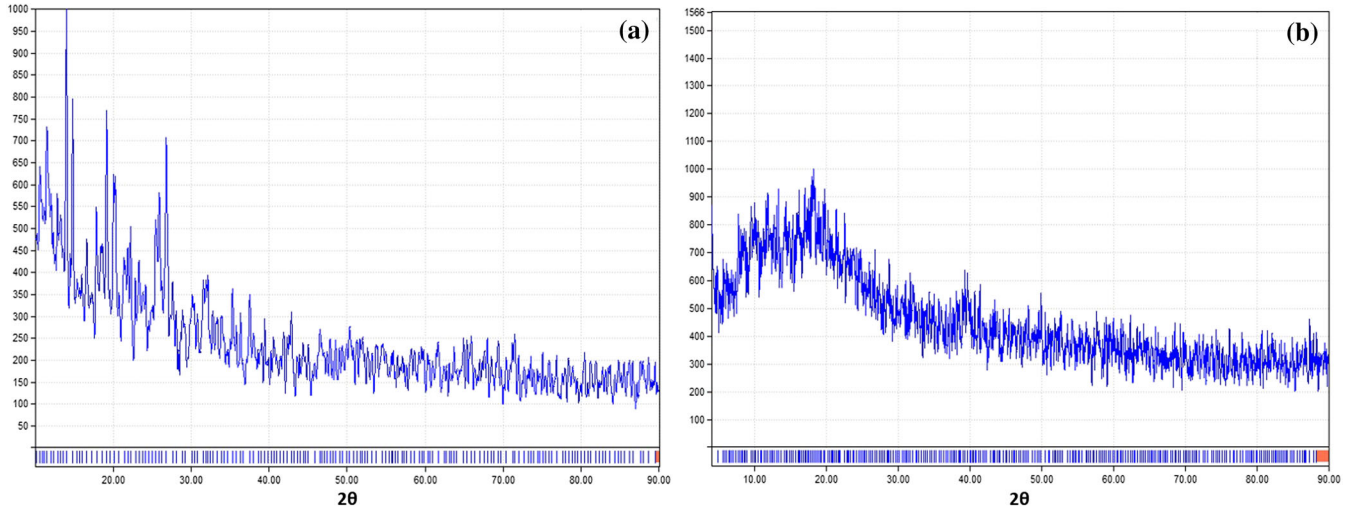

FIGURE 6 XRD patterns of H_2L (a) and Co(II) complex **2** (b)

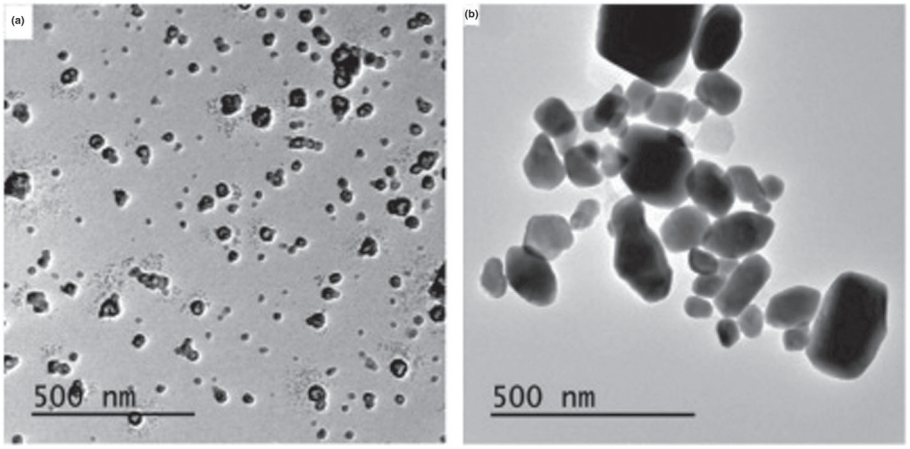

FIGURE 7 TEM micrographs of Cu(II) complex **1** (a) and Co(II) complex **2** (b)

spherical anions in the complexation sphere usually leads to the spherical nature appearing. Furthermore, this may occur as a consequence of the diverse accumulation of various singular particles of polycrystalline character. The aggregation of condensed fine particles may be the reason for the dark areas appearing in the micrographs. The observed particle diameters for all metal complexes were found to be in nanometric range. The particle sizes reached 12.97 nm for complex **1**, 48.64 nm for complex **2**, 68.14 nm for complex **3**, 42.14 nm for complex **4** and 27.62 nm for complex **5**. These nanometric sizes can promote bio-efficiency compared with the bulk analogue. Such an important feature facilitates the permeability through cell membranes of infected cells. These novel nano-sized compounds can be of great interest as a result of their notable properties and having a wide range of prospective technological applications involving catalysis, microelectronics, optics, chemical sensors and bio-sensors.[47]

3.8 | Bio-efficiency studies

3.8.1 | Evaluation of antitumour activity

Chemotherapy is well known as a main approach for localized and metastasized cancer treatment. Moreover, novel synthetic anticancer therapies are indispensable to progress the result for significant numbers of patients who relapse after treatment with the known and current cancer therapeutic agents.[43,48] The aim of our study was to evaluate the anticancer activities of H_2L and complexes **1**–**5** against human breast cancer cell line (MCF-7 cells) and human hepatocellular carcinoma cell line (HepG-2 cells). We selected MCF-7 and HepG-2 because they are the most common among the various types of carcinomas. The anticancer activity and growth inhibitory activities were specified by IC_{50}.[49] IC_{50} refers to the concentration of scanned component which minimizes cell growth (by 50%) applying the same conditions. Every

point was computed as the average of triple experiments and specified as mean ±standard deviation. The obtained values for IC_{50} for all investigated compounds are listed in Table 4. Figure 8 shows the *in vitro* anticancer activity of the organic ligand and compounds **1**–**5** against HepG-2 cell line, compared with the applied standard drug cisplatin. It is clear that most compounds exhibited an inhibition of cell efficacy and an enhanced cytotoxic efficacy against HepG-2 according to the following order: H_2L < complex **5** < complex **3** < complex **2** < complex **4** < complex **1**.

Figure 9 shows the *in vitro* anticancer activity of H_2L and complexes **1**–**5** towards MCF-7 cell line, in comparison with 5-flurouracil (the applied standard drug). It is apparent that most inspected materials displayed an inhibition of cell viability and increased cytotoxic influence towards MCF-7 according to the following order: H_2L < complex **4** < complex **2** < complex **5** < complex **3** < complex **1**. These results indicate that the type of metal ions and the nature of the ligand are the key factors affecting the anticancer efficiency of the metallic compounds.[50,51] The Cu(II) complex exhibited IC_{50} of 3.47 μg ml^{-1} (5.53 μM), greater than that of the well-known standard drug cisplatin (IC_{50} = 3.67 μg ml^{-1} (12.23 μM)), towards HepG-2 cells. The Co(II), Ni(II) and Zn(II) complexes displayed IC_{50} values nearly equivalent to that of the applied standard 5-flurouracil, and the Cu(II) complex exhibited IC_{50} value greater than it against MCF-7 cells. So, these complexes can be considered strong and quite promising anticancer agents.

3.8.2 | Antibacterial and antifungal activities

In vitro antibacterial and antifungal activities of free ligand H_2L and complexes **1**–**5** were screened applying the diffusion agar technique.[23] The examined organisms were chosen as follows: *Salmonella typhimurium* (RCMB 006 (1) ATCC 14028) was selected as a type of Gram-negative bacterium and *Staphylococcus aureus* (RCMB010010) as a type of Gram-positive bacterium. Also, we selected *Candida albicans* (RCMB 005003 (1) ATCC 10231) as a unicellular fungus and *Aspergillus fumigates* (RCMB 002008) as a multicellular fungus. Hence, such selection displays a broad spectrum of examined microorganisms. The obtained results revealed that ligand H_2L is inactive against all tested organisms. The Cu(II) and Co(II) complexes exhibited good activity towards *S. aureus*, within inhibition zones of 9.03 and 10.17 mm, respectively. The Co(II) complex showed high efficiency against *S. typhimurium* with a 13.13 mm inhibition zone. The Ni(II) complex displayed moderate activity against *A. fumigates* with a 10.97 mm inhibition zone. Also, the Cu(II) complex exhibited good activity towards

TABLE 4 *In vitro* anticancer activity of H_2L and compounds **1**–**5** against HepG-2 and MCF-7 cells

Compound	IC_{50} against HepG-2 cells, μg ml^{-1} (μM)	IC_{50} against MCF-7 cells, μg ml^{-1} (μM)
H_2L	189.0 (478.6)	331.0 (838.3)
1	3.47 (5.53)	14.90(23.77)
2	61.80 (113.9)	27.4 (50.53)
3	79.20 (121.9)	25.70 (39.58)
4	28.60 (46.9)	183.0 (300.1)
5	96.90 (168.8)	26.20 (45.64)

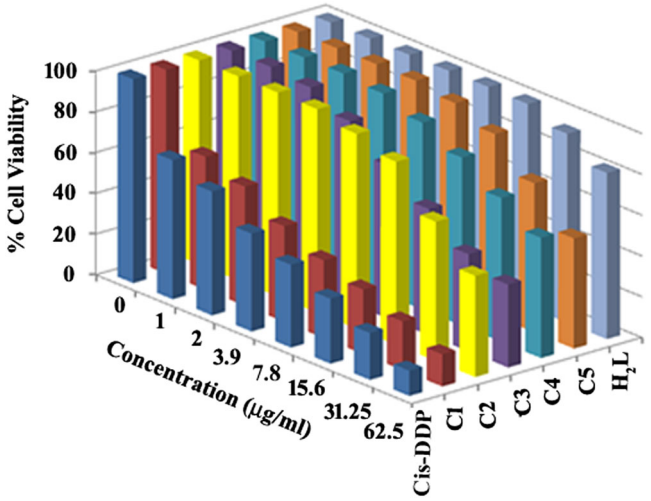

FIGURE 8 *In vitro* anticancer activity of organic ligand and complexes (**C1**–**C5**) against HepG-2 cell line, compared with standard drug cisplatin

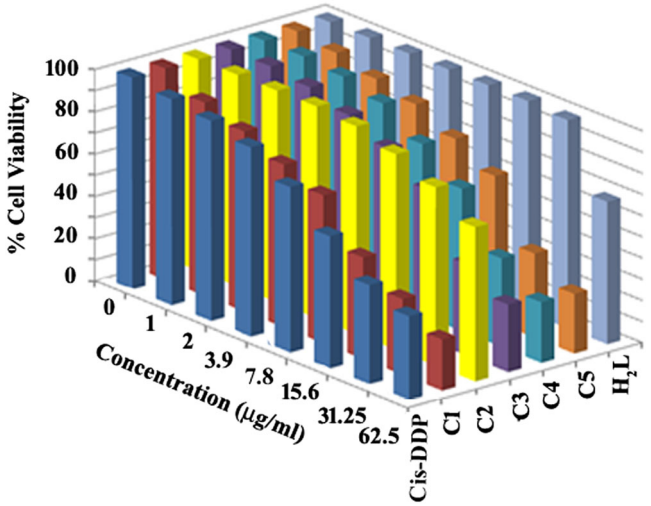

FIGURE 9 *In vitro* anticancer activity of organic ligand and complexes (**C1**–**C5**) against MCF-7 cell line, in comparison with standard 5-flurouracil

C. albicans with a 11.97 mm inhibition zone. Such enhanced activity upon complex formation is best clarified on the basis of Overton's concept[52] and Tweedy's chelation theory.[53] The mode of action may involve hydrogen bond formation between the compounds and the cell centre resulting in an interference with general cell operations. Likewise, the ligand and complexes perhaps perturb the respiration process in the cell and hence prohibit protein formation resulting in limitation in the growth of the organism. Furthermore, the greater antimicrobial efficacy of the complexes in comparison with the free ligand is attributable to the presence of metallic sites. They are more hypersensitive against bacterial cells than free organic compounds.[54] The other compounds were found to be inactive against the tested organisms. The variation in antimicrobial influence of the metal complexes is attributed to the nature of the substituents present in the chelating agent and the nature of metal ions forming the complexes. The mentioned behaviour is attributed to the efficacious charge through d-electrons being decreased by the electron-donating capacity, whilst it increased due to the electron-withdrawing capacity.

3.9 | DNA binding studies

3.9.1 | Electronic absorption spectroscopy studies

Electronic absorption spectroscopy is an essential tool which is applied for evaluating the binding of DNA with compounds and also the extent of binding.[24,55,56] The absorption titration experiments were carried out using constant concentrations of the studied compounds (50 μM) while progressively increasing the concentration of DNA at 25°C (5–45 μM). The absorbance of DNA is cancelled by adding equivalent amounts of DNA to both the tested compounds and reference solutions. The absorption spectra of H_2L and its complexes (**1**–**5**) in the absence and presence of increasing concentrations of DNA are presented in Figures 10 and 11. The intrinsic binding constant (K_b) of compounds with DNA is computed by precisely noting the intensity of the charge transfer bands. In the case of intercalation mode of binding between compounds and DNA, the obvious spectral feature of the band under study is hypochromism with small shift in wavelength; occasionally no shift is observed. This is because the intercalative type of interaction comprises a significant interaction between the aromatic chromophore of the complex compounds and DNA base pairs.[57,58] The extent of absorbance reduction, hypochromism, is ordinarily indicative of the extent of intercalation. The other obvious spectral feature is hyperchromism. Hyperchromism is consistent with the fracturing of the secondary DNA structure.[59,60] The binding ability and extent of binding between H_2L and complexes **1**–**5** and DNA is discussed based on absorbance as a function of added DNA concentration. The data obtained showed that by increasing the concentration of DNA in the range 5–45 μM, the absorption bands of H_2L and complex **4** at 397 and 394 nm exhibited hypochromism of 4.5 and 18.4%, respectively. These data indicated strong association of the compounds with SS-DNA, and it is also more likely that the interaction mode is intercalation. On the other hand, compounds **1**, **2**, **3** and **5** exhibited hyperchromism of 20.3, 31.4, 24.9 and 18.7%, respectively, of the charge transfer bands appearing at 470, 393, 402 and 408 nm, respectively. This spectral change can be indicative of groove binding mode.[61] To illustrate the extent of binding of compounds to DNA quantitatively, K_b was calculated using the following equation:

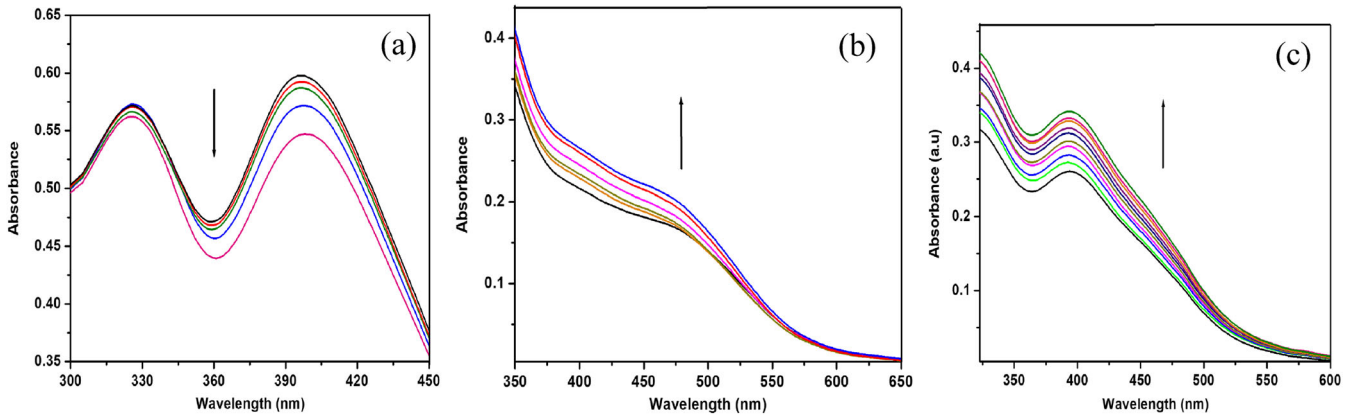

FIGURE 10 Absorption spectra of (a) H_2L, (b) complex **1** and (c) complex **2** upon titration of SS-DNA. Arrows show the absorption change with increasing DNA concentration

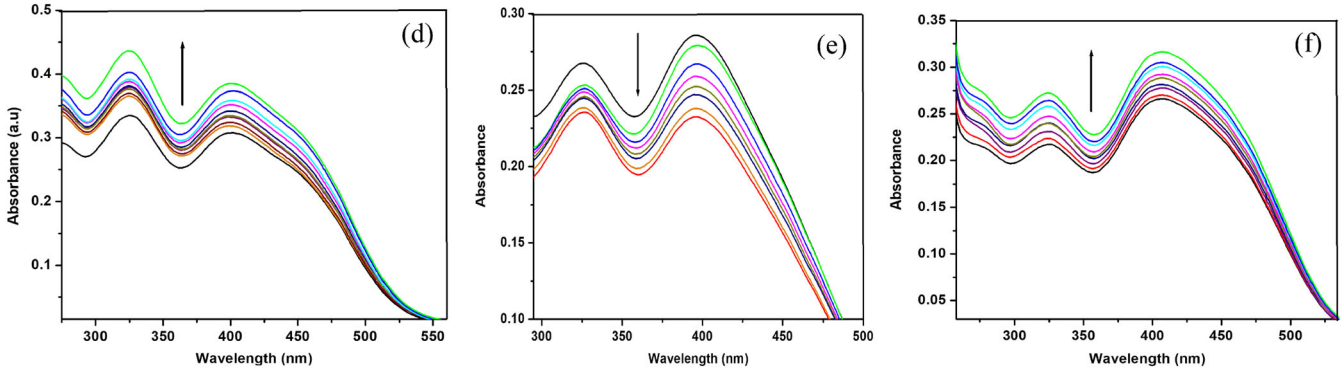

FIGURE 11 Absorption spectra of (d) complex **3**, (e) complex **4** and (f) complex **5** upon titration of SS-DNA. Arrow indicates the absorption change with increasing DNA concentration

$$[\mathrm{DNA}]/(\varepsilon_a - \varepsilon_f) = [\mathrm{DNA}]/(\varepsilon_b - \varepsilon_f) + 1/[K_b(\varepsilon_b - \varepsilon_f)]$$

where [DNA] is the concentration of DNA solution in base pairs. The absorption coefficient ε_a equals A_{obs}/[compound] while ε_f and ε_b refer to the extinction coefficients of the unbounded and the compound in a fully bound state to DNA, respectively. A plot of [DNA]/($\varepsilon_a - \varepsilon_f$) versus [DNA] is a straight line with slope = 1/($\varepsilon_b - \varepsilon_f$) and intercept = $1/K_b(\varepsilon_b - \varepsilon_f)$; K_b is calculated from the ratio of slope to intercept. Analyses of the calculated K_b values of the studied compounds illustrate that the examined compounds have moderate binding ability when these values are compared with those for ethidium bromide which is a well-known intercalator.[62] The obtained values of K_b were found to be 1.98×10^4, 1.77×10^4, 1.3×10^4, 1.2×10^4, 1.4×10^3 and 7.7×10^3 for H_2L and complexes **1**, **2**, **3**, **4** and **5**, respectively.

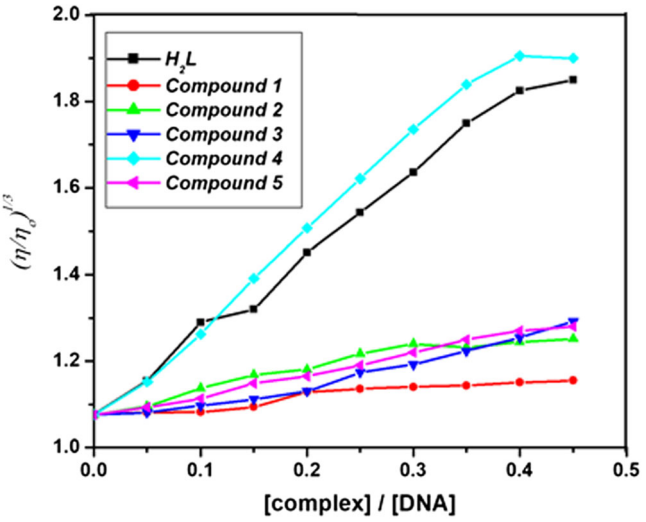

FIGURE 12 Effect of increasing concentrations of H_2L and complexes **1**–**5** on viscosity of SS-DNA

3.9.2 | Viscosity measurements

Optical tools provide substantial, but not sufficient, evidence to support the intercalative type of interaction between compounds and DNA. A hydrodynamic tool, like viscosity, that introduces large accuracy to any change in DNA length, is probably an influential tool in order to evaluate the binding mode between tested compounds and DNA. The viscosity of DNA solutions was recorded using different dilutions of ligand H_2L and compounds**1**–**5** using a constant concentration of DNA solution. Figure 12 shows the influence of increasing concentrations of the compounds on DNA viscosity. Viscosity measurement of DNA is regarded a classic way to assess the type of DNA interaction in solution. Under the normal conditions ethidium bromide, as a known intercalator, usually results in a considerable enhancement in DNA viscosity which results from the increase in the distance between the intercalation site base pairs that results in a final augmentation in the DNA length,[63] as obvious in Figure 12. For H_2L and complex **4**, the obtained results suggest that the compounds can intercalate among the adjacent DNA base pairs, resulting in elongation in the double helix and subsequently increasing the DNA viscosity. This increase in the viscosity by adding increasing amounts of the tested compounds strongly suggests the intercalation binding mode. For complexes **1**–**3** and **5**, the relative viscosity of the DNA solution was almost unchanged or increased slowly over the entire tested range when compared with H_2L and complex **4**, which suggests that the interactions between these compounds and DNA may be via electrostatic forces of groove binding type.

4 | CONCLUSIONS

A novel azo dye ligand has been synthesized in addition to its nano-sized divalent Cu, Co, Ni, Mn and Zn complexes. The structures and geometries of the synthesized

compounds have been confirmed using various analytical and spectroscopic tools (i.e. elemental analysis, FT-IR spectra, thermal analysis, magnetic moment measurements and UV–visible and ESR spectra). For the metal complexes, elemental and thermal analyses confirmed the formation of the Cu(II), Ni(II) and Mn(II) complexes in a molar ratio 1:2 (L:M), while the Co(II) and Zn(II) complexes are formed in a 1:1 (M:L) ratio. The FT-IR spectral studies illustrated that the ligand binds to the metal ions through the phenolic hydroxyl oxygen, azo nitrogen, sulfonamide oxygen and/or thiazole nitrogen. UV–visible and ESR spectra in addition to magnetic moment measurements confirmed tetrahedral geometry around the metal centres. XRD patterns indicated the crystalline nature of H_2L and amorphous nature of its complexes. The nano-sized nature of the metal complexes has been confirmed from TEM images. The investigated compounds were screened for their antitumour, antibacterial and antifungal activities comparing with well-known standard drugs to evaluate their potential therapeutic applications. The antitumour activity results indicated that the Cu(II) complex exhibited IC_{50} of 3.47 μg ml^{-1} (5.53 μM) against hepatocellular carcinoma cells, which means that it is a more potent anticancer drug than the standard cisplatin (IC_{50} = 3.67 μg ml^{-1} (12.23 μM)). Furthermore, the Co(II), Ni(II), Cu(II) and Zn(II) complexes displayed IC_{50} greater than that of standard anticancer agent 5-flurouracil towards breast carcinoma cells. Hence, these complexes can be considered promising anticancer drugs. The mode of binding of the complexes with SS-DNA has been investigated through electronic absorption titration and viscosity studies. The obtained results confirmed that H_2L and complex **4** bind to DNA by intercalation binding mode while the binding modes of DNA to the other compounds are via electrostatic forces or groove binding mode.

ACKNOWLEDGEMENTS

This paper contains the results and findings of a research project that is funded by King Abdulaziz City for Science and Technology (KACST) under grant no. 37-175.

ORCID

Fawaz A. Saad https://orcid.org/0000-0003-4910-361X
Hoda A. El-Ghamry https://orcid.org/0000-0003-4737-1012

REFERENCES

[1] H. Rehman, A. Qadir, H. A. Shad, Z. I. Khan, *Med. Chem. (Los Angeles)* **2017**, *7*, 252.

[2] Y. Kwon, J. Song, H. Lee, E.-Y. Kim, K. Lee, S. K. Lee, S. Kim, *J. Med. Chem.* **2015**, *58*, 7749.

[3] A. Agudo-López, E. Prieto-García, J. Alemán, C. Pérez, C. V. Díaz-García, L. Parrilla-Rubio, S. Cabrera, C. Navarro-Ranninger, H. Cortés-Funes, J. A. López-Martín, M. T. Agulló-Ortuño, *Mol. Cancer* **2017**, *16*(1), 45.

[4] K. G. Samper, S. C. Marker, P. Bayón, S. N. MacMillan, I. Keresztes, O. Palacios, J. J. Wilson, *J. Inorg. Biochem.* **2017**, *174*, 102.

[5] H. El-Ghamry, K. Sakai, S. Masaoka, K. El-Baradie, R. Issa, *J. Coord. Chem.* **2012**, *65*, 780.

[6] M. Gaber, K. El-Baradie, Y. El-Sayed, *Spectrochim. Acta A* **2008**, *69*, 534.

[7] T. K. Misra, D. Das, C. Sinha, P. Ghosh, C. K. Pal, *Inorg. Chem.* **1998**, *37*, 1672.

[8] R. Pingaew, V. Prachayasittikul, A. Worachartcheewan, C. Nantasenamat, S. Prachayasittikul, S. Ruchirawat, V. Prachayasittikul, *Eur. J. Med. Chem.* **2015**, *103*, 446.

[9] A. Z. El-Sonbati, A. A. El-Bindary, R. M. Ahmed, *J. Solution Chem.* **2003**, *32*, 617.

[10] A. Z. El-Sonbati, M. A. Diab, M. S. El-Shehawy, M. Moqbal, *Spectrochim. Acta A* **2010**, *75*, 394.

[11] A. Z. El-Sonbati, R. M. Issa, A. M. Abd El-Gawad, *Spectrochim. Acta A* **2007**, *68*, 134.

[12] J. Casanova, G. Alzuet, S. Ferrer, J. Borrás, S. García-Granda, E. Perez-Carreño, *J. Inorg. Biochem.* **1993**, *51*, 689.

[13] F. A. Saad, A. M. Khedr, *J. Mol. Liq.* **2017**, *231*, 572.

[14] F. A. Saad, A. M. Khedr, *Bulg. Chem. Commun.* **2015**, *47*, 654.

[15] H. Li, G.-H. Lee, S.-M. Peng, *Inorg. Chem. Commun.* **2003**, *6*, 1.

[16] R. M. Issa, A. M. Khedr, A. Tawfik, *Synth. React. Inorg.Met.-Org. Chem.* **2004**, *34*, 1087.

[17] P. Nordell, P. Lincoln, *J. Am. Chem. Soc.* **2005**, *127*, 9670.

[18] A. T. Chaviara, P. J. Cox, K. H. Repana, A. A. Pantazaki, K. T. Papazisis, A. H. Kortsaris, D. A. Kyriakidis, G. S. Nikolov, C. A. Bolos, *J. Inorg. Biochem.* **2005**, *99*, 467.

[19] A. M. Pyle, J. P. Rehmann, R. Meshoyrer, C. V. Kumar, N. J. Turro, J. K. Barton, *J. Am. Chem. Soc.* **1989**, *111*, 3051.

[20] B. Macías, M. V. Villa, R. Lapresa, G. Alzuet, J. Hernández-Gil, F. Sanz, *J. Inorg. Biochem.* **2012**, *115*, 64.

[21] T. Mosmann, *J. Immunol. Methods* **1983**, *65*, 55.

[22] S. M. Gomha, S. M. Riyadh, E. A. Mahmmoud, M. M. Elaasser, *Chem. Heterocycl. Comp.* **2015**, *51*, 1030.

[23] A. C. Scott, Laboratory control of antimicrobial therapy, in *Practical Medical Microbiology*, 13th ed. (Eds: J. G. Collee, J. P. Duguid, A. G. Fraser, B. P. Marmion), Churchill Livingstone, Edinburgh **1981**.

[24] M. Gaber, N. A. El-Wakiel, H. El-Ghamry, S. K. Fathalla, *J. Mol. Struct.* **2014**, *1076*, 251.

[25] W. J. Geary, *Coord. Chem. Rev.* **1971**, *7*, 81.

[26] K. Nakamoto, *Infrared Spectra of Inorganic and Coordination Compounds*, Wiley, New York **1986**.

[27] K. Y. El-Baredie, *Monatsh. Chem.* **2005**, *136*, 1139.

[28] K. El-Baradie, R. El-Sharkawy, H. El-Ghamry, K. Sakai, *Spectrochim. Acta A* **2014**, *121*, 180.

[29] G. Q. Zhong, J. Shen, Q. Y. Jiang, Y. Q. Jia, M. J. Chen, Z. P. Zhang, *J. Therm. Anal. Calorim.* **2008**, *92*, 607.

[30] J. R. Allan, W. C. Geddes, C. S. Hindle, A. E. Orr, *Thermochim. Acta* **1989**, *153*, 249.

[31] M. Badea, A. Emandi, D. Marinescu, E. Cristurean, R. Olar, A. Braileanu, P. Budrugeac, E. Segal, *J. Therm. Anal. Calorim.* **2003**, *72*, 525.

[32] A. W. Coats, J. P. Redfern, *Nature* **1964**, *201*, 68.

[33] A. Frost, R. Pearson, *Kinetics and Mechanism*, John Wiley, New York **1961**.

[34] U. El-Ayaan, I. Kenawy, Y. A. El-Reash, *Spectrochim. Acta A* **2007**, *68*, 211.

[35] S. Gupta, S. Pal, A. K. Barik, A. Hazra, S. Roy, T. N. Mandal, S.-M. Peng, G.-H. Lee, M. Salah El Fallah, J. Tercero, S. K. Kar, *Polyhedron* **2008**, *27*, 2519.

[36] P. N. Patel, D. J. Patel, H. S. Patel, *Appl. Organometal. Chem.* **2011**, *25*, 454.

[37] A. A. Osowole, E. J. Akpan, *Eur. J. Appl. Sci.* **2012**, *4*, 14.

[38] M. M. Al-Ne'aimi, M. M. Al-Khuder, *Spectrochim. Acta A* **2013**, *105*, 365.

[39] D. X. West, A. Nassar, F. A. El-Saied, M. I. Ayad, *Transition Met. Chem.* **1998**, *23*, 423.

[40] W. Al Zoubi, A. A. S. Al-Hamdani, S. D. Ahmed, Y. G. Ko, *J. Phys. Org. Chem.* **2018**, *31*, 3752.

[41] D. N. Kumar, B. S. Garg, *Spectrochim. Acta A* **2006**, *64*, 141.

[42] T. M. A. Ismail, *J. Coord. Chem.* **2005**, *58*, 141.

[43] A. A. Fahem, *Spectrochim. Acta A* **2012**, *88*, 10.

[44] J. S. Ritch, T. Chivers, K. Ahmad, M. Afzaal, P. O'Brien, *Inorg. Chem.* **2010**, *49*, 1198.

[45] F. A. Saad, M. G. Elghalban, N. El-Metwaly, H. El-Ghamry, A. M. Khedr, *Appl. Organometal. Chem.* **2017**, *31*, e3721.

[46] J. K. Hui, M. J. MacLachlan, *Coord. Chem. Rev.* **2010**, *254*, 2363.

[47] A. Salimi, J. R. Halla, S. Soltanian, *Biophys. Chem.* **2007**, *130*, 122.

[48] A. S. Sultan, H. Brim, Z. A. Sherif, *Cancer Sci.* **2008**, *2*, 272.

[49] S. H. Etaiw, S. A. Amer, M. M. El-Bendary, *J. Inorg. Organometal. Polym. Mater.* **2011**, *21*, 662.

[50] X. Riera, V. Moreno, C. J. Ciudad, V. Noe, M. Font-Bardía, X. Solans, *Bioinorg. Chem. Appl.* **2007**, *2007*, 1.

[51] M. Gaber, A. M. Khedr, M. Elsharkawy, *Appl. Organometal. Chem.* **2017**, *31*, e3885.

[52] A. Kulkarni, S. A. Patil, P. S. Badami, *Eur. J. Med. Chem.* **2009**, *44*, 2904.

[53] K. N. Thimmaiah, W. D. Lloyd, G. T. Chandrappa, *Inorg. Chim. Acta* **1985**, *106*, 81.

[54] M. A. Phanib, S. D. Dhumwad, *Transit. Met.Chem.* **2007**, *32*, 1117.

[55] T. Hirohama, Y. Kuranuki, E. Ebina, T. Sugizaki, H. Arii, M. Chikira, P. T. Selvi, M. Palaniandavar, *J. Inorg. Biochem.* **2005**, *99*, 1205.

[56] A. Z. El-Sonbati, M. A. Diab, A. A. El-Bindary, M. M. Ghoneim, M. T. Mohesien, M. K. Abd El-Kader, *J. Mol. Liq.* **2016**, *215*, 711.

[57] T. R. Li, Z. Y. Yang, B. D. Wang, D. D. Qin, *Eur. J. Med. Chem.* **2008**, *43*, 1688.

[58] B. Wang, Z. Y. Yang, P. Crewdson, D. Wang, *J. Inorg. Biochem.* **2017**, *101*, 1492.

[59] N. Chitrapriya, V. Mahalingam, M. Zeller, K. Natarajan, *Inorg. Chim. Acta* **2010**, *363*, 3685.

[60] F. Firdaus, K. Fatma, M. Azam, S. Khan, A. Khan, M. Shakir, *Transit. Met. Chem.* **2008**, *33*, 467.

[61] R. Vijayalakshmi, M. Kanthimathi, V. Subramanian, B. Nair, *Biochem. Biophys. Acta* **2000**, *1475*, 157.

[62] M. J. Waring, *J. Mol. Biol.* **1965**, *13*, 269.

[63] F. H. Li, G. H. Zhao, H. X. Wu, H. Lin, X. X. Wu, S. R. Zhu, H. K. Lin, *J. Inorg. Biochem.* **2006**, *100*, 36.

SUPPORTING INFORMATION

Additional supporting information may be found online in the Supporting Information section at the end of the article.

How to cite this article: Saad FA, El-Ghamry HA, Kassem MA. Synthesis, structural characterization and DNA binding affinity of new bioactive nano-sized transition metal complexes with sulfathiazole azo dye for therapeutic applications. *Appl Organometal Chem*. 2019;33: e4965. https://doi.org/10.1002/aoc.4965